

Control of Lower-Limb Overturning Circulation in the Southern Ocean by Diapycnal Mixing and Mesoscale Eddy Transfer

TAKA ITO

Department of Atmospheric Science, Colorado State University, Fort Collins, Colorado

JOHN MARSHALL

Program in Atmospheres, Oceans and Climate, Department of Earth Atmospheric and Planetary Science, Massachusetts Institute of Technology, Cambridge, Massachusetts

(Manuscript received 10 July 2007, in final form 26 May 2008)

ABSTRACT

A simple model is developed of the lower limb of the meridional overturning circulation in the Southern Ocean based on residual-mean theory. It is hypothesized that the strength of the lower-limb overturning (Ψ) is strongly controlled by the magnitude of abyssal diapycnal mixing (κ) and that of mesoscale eddy transfer (K). In particular, it is argued that $\Psi \propto \sqrt{\kappa K}$. The scaling and associated theory find support in a suite of sensitivity experiments with an idealized ocean general circulation model. This study shows that intense diapycnal mixing is required to close the buoyancy budget of the lower-limb overturning circulation, in contrast to the upper limb, where air–sea buoyancy fluxes can provide the required diabatic forcing.

1. Introduction

The abyssal ocean contains by far the largest volume of waters in the global ocean, dominating the oceanic inventory of heat, nutrients, carbon, and other geochemical tracers. The deep meridional overturning circulation ventilates the deep waters from a few selected regions in the northern North Atlantic and the polar Southern Ocean. Our focus in this paper is on the deep overturning circulation of the Southern Ocean.

The circulation of the Southern Ocean is dominated by the Antarctic Circumpolar Current (ACC), whose circulation is characterized by zonal jets forced by the surface wind and steered by bottom topography. Recently, dynamical theory describing the upper limb of the meridional overturning circulation has been developed by the application of residual-mean theory, in which the balance between Ekman transport and the mesoscale eddies plays a fundamental role in setting the stratification and overturning circulation (Karsten et al. 2002; Marshall and Radko 2003, hereafter MR03, 2006;

Bryden and Cunningham 2003; Olbers and Visbeck 2005). The upper limb includes the upwelling of Circumpolar Deep Water, northward surface residual flow, and subsequent formation and subduction of Antarctic Intermediate Water and Subantarctic Mode Water. In the upper limb, air–sea buoyancy flux can provide the necessary diabatic forcing for water mass transformation (Speer et al. 2000) while the interior circulation is likely to be nearly adiabatic and oriented along isopycnal surfaces (Webb and Suginohara 2001; MR03).

In contrast, recent field experiments discovered intense diapycnal mixing in the abyssal Southern Ocean (Heywood et al. 2002; Naveira Garabato et al. 2004, 2007). Near the bottom topography, diapycnal diffusivity is observed to exceed the small values of the upper ocean by a factor of 100 to 1000. These observations imply that the buoyancy balance of the lower limb circulation is fundamentally different from that of the upper limb. What is the impact of this intense mixing on lower limb circulation? Box inverse models have resulted in a wide range of estimates for the overturning circulation (Ganachaud and Wunsch 2000; Sloyan and Rintoul 2001), but such calculations may be compromised because they do not take into account the vigorous eddy field of the Southern Ocean. Moreover, it is

Corresponding author address: Taka Ito, Department of Atmospheric Science, 1371 Campus Delivery, Colorado State University, Fort Collins, CO 80523-1371.
E-mail: ito@atmos.colostate.edu

difficult to constrain the lower limb circulation by limited hydrographic data or directly observe deep water formation that occurs in narrow regions near the continental shelves around Antarctica.

In this paper, we postulate that diapycnal mixing and mesoscale eddy transfer in the abyss play an important role in the buoyancy balance of the lower-limb circulation, and we develop a simple, zonally averaged theory relating the strength of the overturning circulation to mixing rates as summarized in the abstract. The theory is developed in section 2. In section 3, we use a general circulation model configured in an idealized setting to test the theory in a suite of sensitivity experiments. In section 4, we summarize and discuss the implications of our results.

2. Theory

In this section, we develop a simple model of the circulation of the lower limb based on the momentum and buoyancy balance of the Southern Ocean. The model is based on the residual-mean framework of Andrews and McIntyre (1976) in which the net effect of Eulerian-mean ($\bar{\Psi}$) and eddy-induced circulation (Ψ^*) determine the residual streamfunction for the overturning circulation:

$$\Psi_{\text{res}} = \bar{\Psi} + \Psi^*. \tag{1}$$

Our model builds on the “*f*-plane” theory of the upper-limb circulation (MR03).¹ Here we extend MR03 to include the effects of diapycnal mixing and a simple representation of bottom topography. We first discuss the residual-mean buoyancy and momentum balance in the Southern Ocean and go on to derive a simple scaling that relates the strength of the lower limb circulation to diapycnal diffusivity, mesoscale eddy transfer, and the forcing fields.

a. Buoyancy and momentum balances

1) BUOYANCY

We adopt a streamwise-average view of the ACC and integrate the time-averaged residual buoyancy equation along the mean streamlines circumnavigating the globe to obtain, using a Cartesian coordinate system in which *y* and *z* point, respectively, northward and upward (see MR03 for more details):

$$u_{\text{res}} \frac{\partial \bar{b}}{\partial y} + w_{\text{res}} \frac{\partial \bar{b}}{\partial z} = \frac{\partial}{\partial z} \left(\kappa \frac{\partial \bar{b}}{\partial z} \right). \tag{2}$$

¹ See also Marshall and Radko (2006), who reviewed the role of the β effect in the dynamics of the upper limb and extended the theory of MR03.

Here, $\mathbf{v}_{\text{res}} = \bar{\mathbf{v}} + \mathbf{v}^*$ is the residual velocity, the sum of the Eulerian-mean $\bar{\mathbf{v}}$ and eddy-induced transport

$$\mathbf{v}^* = (u^*, w^*) = (-\Psi_z^*, \Psi_y^*),$$

expressed in terms of an eddy-induced streamfunction; thus,

$$\Psi^* = \frac{\overline{v'b'}}{\bar{b}_z}. \tag{3}$$

Note that in Eq. (2) the role of the eddies—and this is the whole point of residual-mean theory—have been subsumed in to the definition of the advecting velocity \mathbf{v}_{res} , assuming that the eddy fluxes do not have a component across time-mean buoyancy surfaces, that is, that they are entirely “skew.”

If we consider Eq. (2) moving along a buoyancy surface, where \bar{b} is constant, then we have [see Eq. (13) of Karsten and Marshall (2002) and derivation therein]

$$\frac{d\Psi_{\text{res}}}{d\bar{y}} = \frac{\partial}{\partial z} \left(\kappa \frac{\partial \bar{b}}{\partial z} \right) \frac{1}{\sqrt{\bar{b}_y^2 + \bar{b}_z^2}} \approx \frac{1}{\bar{b}_z} \frac{\partial}{\partial z} \left(\kappa \frac{\partial \bar{b}}{\partial z} \right), \tag{4}$$

where the simplification arises when, as is almost always the case, $\bar{b}_z^2 \gg \bar{b}_y^2$. Here, \bar{y} is the distance traveled along a \bar{b} surface, which is almost identical to *y* because slopes of \bar{b} surfaces are small. This relationship can be used to diagnose Ψ_{res} given a distribution of \bar{b} and κ . Karsten and Marshall (2002) employed Eq. (4) by integrating down from the surface using an observed \bar{b} distribution and an assumed constant value of κ . In a theoretical calculation, MR03 calculated the upper-limb circulation using the method of characteristics in the limit case of $\kappa = 0$ in which, consequently, Ψ_{res} is constant along \bar{b} .

Figure 1 shows the distribution of zonally averaged buoyancy in the Southern Ocean. Note that isopycnal surfaces intersect bottom topography in the latitudes of the Antarctic Circumpolar Current (45°–65°S). Now, Eq. (4) can be integrated up along \bar{b} surfaces to obtain an explicit expression for Ψ_{res} in terms of κ . Starting from the position where \bar{b} intersects the bottom topography ($\bar{y} = \bar{y}_{\text{bottom}}$) and moving in to the interior ocean along \bar{b} and setting Ψ_{res} to zero on the boundary because no flow can cross it, we obtain

$$\Psi_{\text{res}}(\bar{y}, \bar{b}) = \int_{\bar{y}_{\text{bottom}}}^{\bar{y}} \frac{1}{\bar{b}_z} \frac{\partial}{\partial z} \left(\kappa \frac{\partial \bar{b}}{\partial z} \right) d\bar{y}, \tag{5}$$

where $\Psi_{\text{res}}(\bar{y}, \bar{b})$ represents the mass transport between the isopycnal layer \bar{b} and the bottom, and the integral must be evaluated along a constant \bar{b} surface. Negative Ψ_{res} indicates equatorward mass flux. Thus, if $\kappa = 0$, $\Psi_{\text{res}} = 0$ along the entire \bar{b} surface and there can be no mass transport along and across \bar{b} . This condition will

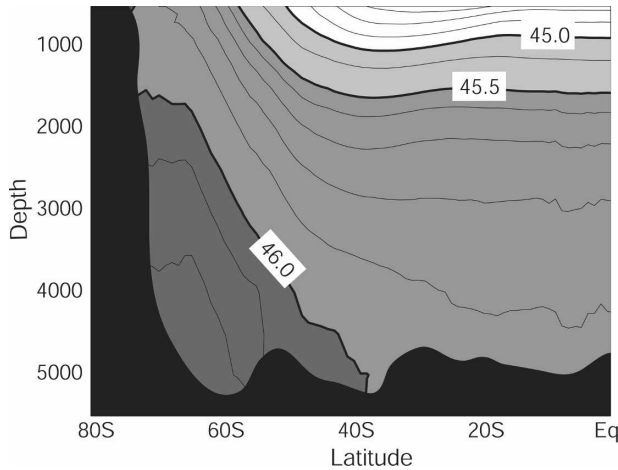


FIG. 1. Zonally averaged potential density (σ_4) based on the *World Ocean Atlas 2001* (Conkright et al. 2002). Above the density level 45.5 ($\sigma_4 < 45.5$) the contour interval is 0.25 kg m^{-3} . Between the density level 44.5 and 46.0 ($45.5 < \sigma_4 < 46.0$) the contour interval is 0.10 kg m^{-3} . Below the density level 46.0 ($46.0 < \sigma_4$) the contour interval is 0.05 kg m^{-3} .

not allow any equatorward transport of Antarctic Bottom Water (AABW) and, of course, tells us that diapycnal mixing is crucial in supporting deep meridional overturning circulation.

2) MOMENTUM

The zonal and time-averaged streamwise momentum balance can be written as follows, neglecting horizontal eddy momentum fluxes (which are known to be small on a large scale in the ACC as discussed in Marshall 1997):

$$-\rho_0 f \bar{v} = -\frac{\Delta p}{L_x} + \frac{\partial \tau}{\partial z}, \quad (6)$$

where f is the Coriolis parameter, ρ_0 is the mean density of water, \bar{v} is the Eulerian-mean cross-stream velocity, Δp is the pressure drop across topography, L_x is the distance around the globe following the mean path of the ACC, and τ is the applied stress having a value τ_s , the wind stress, at the surface. The pressure gradient term vanishes above the levels that are not blocked by the topography—that is, above ridges. Below the depth of ridges, however ($z < -H_T$; see Fig. 2), the pressure difference across them plays a zero-order role in the momentum budget.

Vertically integrating Eq. (6) from the bottom to the surface ($-H < z < 0$), we find a balance between the surface wind stress and the mountain drag across topographic ridges.

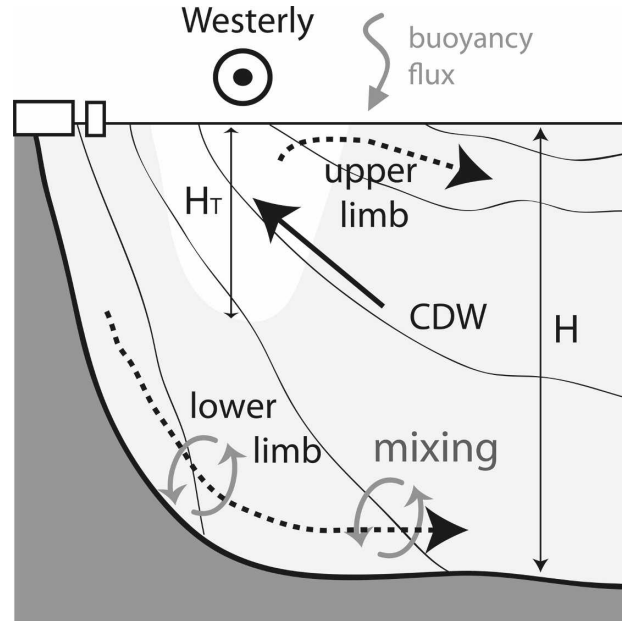


FIG. 2. The zonally unblocked, circumpolar region in the Southern Ocean is represented schematically by the white area with depth H_T . The total depth of the water column is H . The thick, solid arrows represent the upwelling of Circumpolar Deep Water driven by the residual-mean circulation. The dashed line represents the upper- and lower-limb circulations. The advective buoyancy transport of the lower-limb circulation is balanced by the intense diapycnal mixing in the deep Southern Ocean represented by the gray arrows; in contrast, buoyancy transport by the upper limb is primarily balanced by air-sea fluxes.

Exploiting this balance, we can parameterize the zonal pressure gradient thus:

$$\Delta p = L_x \frac{\tau_s}{H - H_T}, \quad (7)$$

and the corresponding Eulerian-mean circulation becomes

$$\bar{\Psi} = \begin{cases} -\frac{\tau_s}{\rho_0 f} & (z > -H_T), \\ -\frac{\tau_s}{\rho_0 f} \left(\frac{H+z}{H-H_T} \right) & (z < -H_T). \end{cases} \quad (8)$$

Replacing v with $(v_{\text{res}} - v^*)$ in Eq. (6), the residual momentum balance can be written

$$-\rho_0 f v_{\text{res}} = -\frac{\Delta p}{L_x} + \frac{\partial \tau}{\partial z} + \rho_0 f \frac{\partial \Psi^*}{\partial z}. \quad (9)$$

Note that the vertical momentum flux through interfacial drag (Johnson and Bryden 1989) is directly related to Ψ^* , as discussed in MR03. Eastward momentum input from the surface (τ_s) is transferred vertically to depth through this interfacial drag ($\rho_0 f \Psi^*$), where it is

balanced by mountain drag $[-\Delta p L_x^{-1}(H - H_T)]$. Such a balance has been established in observations (Phillips and Rintoul 2000) and in numerical simulations (Ivchenko et al. 1996; Gille 1997).

b. Scaling for Ψ_{res}

We now develop scaling for the dependence of Ψ_{res} on diapycnal diffusivity κ by exploiting our residual buoyancy and momentum balances. The predicted scalings will be tested in an ocean general circulation model in section 3.

1) SIMPLIFIED SOLUTION

We assume a mean buoyancy field of the form

$$\bar{b} = \tilde{b}(y)e^{\frac{z}{z_0}}, \tag{10}$$

where z_0 is an e -folding scale. Note that $z = 0$ at the surface and z decreases downward, and so Eq. (10) represents a decay moving down in the water column. Then, Eq. (5) can be written

$$\Psi_{res}(\bar{y}, \bar{b}) = \left(\frac{\kappa}{z_0} + \frac{\partial \kappa}{\partial z} \right) (\bar{y} - \bar{y}_{bottom}). \tag{11}$$

We see that the y dependence of \bar{b} naturally cancels out and Ψ_{res} becomes a linear function of y : the overturning circulation is set by the vertical variation of κ and z_0 , which specifies the abyssal stratification.

To derive our scaling, we further assume that κ is a uniform constant and evaluate the magnitude of Ψ_{res} at a particular distance L from the incrop \bar{y}_{bottom} . For a \bar{b} of the form Eq. (10), we may write

$$s_\rho = -\frac{\bar{b}_y}{\bar{b}_z} = -\frac{\tilde{b}_y}{\tilde{b}} z_0 = \alpha \frac{z_0}{L}, \tag{12}$$

where $\alpha = \Delta \tilde{b} / \tilde{b}$ is a scale factor (typically much less than one) between z_0/L and the slope of \bar{b} surfaces. Equation (11) becomes, noting that $L = |\bar{y} - \bar{y}_{bottom}|$,

$$\Psi_{res} = \alpha \frac{\kappa}{s_\rho}. \tag{13}$$

Another expression for Ψ_{res} can be obtained directly from its definition [Eq. (1)]:

$$\Psi_{res} = \bar{\Psi} + K s_\rho, \tag{14}$$

where Ψ^* has been parameterized following Gent and McWilliams (1990, hereafter GM90) and K is an eddy diffusivity for buoyancy. Equations (13) and (14) yield a quadratic equation for s_ρ whose negative root is the appropriate choice in the Southern Ocean. The implied residual circulation is given by

$$\Psi_{res} = \frac{\bar{\Psi}}{2} (1 - \sqrt{1 + \phi}), \tag{15}$$

where ϕ is a dimensionless, positive-definite quantity given by

$$\phi \equiv \frac{4\alpha\kappa K}{\bar{\Psi}^2}. \tag{16}$$

Equation (15) suggests that the strength of the lower limb depends on ϕ , which itself depends on the diapycnal diffusivity (κ), eddy transfer coefficient [K as defined in Eq. (14)], and the Eulerian circulation, set by the wind stress ($\bar{\Psi}$). The nondimensional parameter ϕ essentially reflects the relative magnitude of Ψ^* and $\bar{\Psi}$. For example, $\phi \rightarrow 0$ implies that κK is very small compared to $\bar{\Psi}^2$, yielding a vanishingly small Ψ_{res} . A stronger Eulerian-mean circulation (i.e., due to a stronger wind stress τ_s) yields a larger ϕ , and hence leads to a weakening of Ψ_{res} . When ϕ is sufficiently large ($\phi \gg 1$), our scaling predicts that the strength of the lower limb circulation is proportional to $\sqrt{\kappa K}$ and independent of $\bar{\Psi}$:

$$\Psi_{res} \sim -\sqrt{\kappa K}. \tag{17}$$

An increase in the diapycnal diffusivity (κ) and/or eddy diffusivity (K) implies a stronger residual-mean circulation (i.e., stronger export of AABW). In the following section, we perform a series of sensitivity experiments to evaluate these theoretical predictions in the context of numerical experiments with a more detailed model.

2) TYPICAL NUMBERS

The strength of the lower-limb circulation is essentially controlled by ϕ , which depends on κ , K , and τ_s as shown in Eqs. (15) and (16). Here, we estimate the magnitude of ϕ based on typical Southern Ocean conditions. The westerly wind stress is on the order of $\tau = 0.1 \text{ N m}^{-2}$, and the Coriolis parameter is $f = -10^{-4} \text{ s}^{-1}$. Considering Eq. (8), the magnitude of ϕ depends on the depth at which $\bar{\Psi}$ is evaluated. Here, we simply average $\bar{\Psi}$ over the bottom 500 m of the model domain, leading to the estimate of $\bar{\Psi} = 0.1 \text{ m}^2 \text{ s}^{-1}$, which is about 10% of the upper ocean values of $\bar{\Psi}$ due to the effect of bottom topography. The climatological buoyancy distribution suggests z_0 on the order of 10^3 m , L on the order of 10^6 m , and α on the order of 0.3.

The value of ϕ essentially reflects the relative magnitude of κK and $\bar{\Psi}^2$. We first make a rough estimate of the cross- and along-isopycnal diffusivities. In the abyss, diapycnal diffusivity may be on the order of $\kappa = 10^{-4} \text{ m}^2 \text{ s}^{-1}$ (Munk 1966), and isopycnal diffusivity may be on the order of $500 \text{ m}^2 \text{ s}^{-1}$. Combining these param-

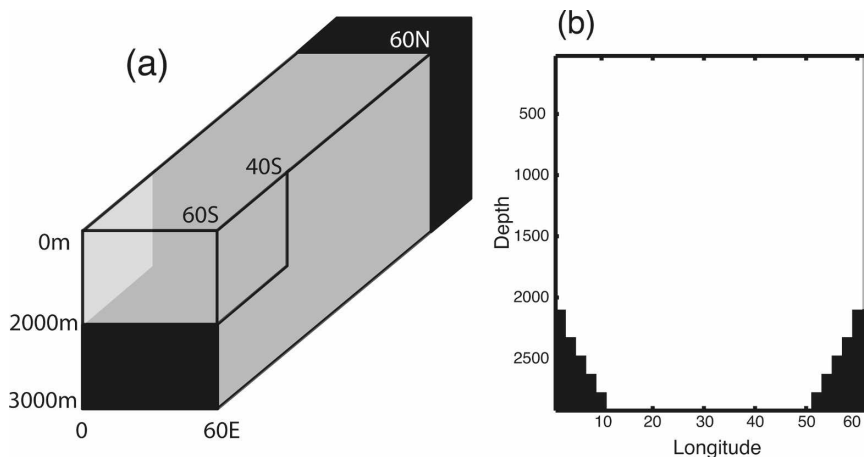


FIG. 3. Configuration of idealized numerical ocean model. (a) Model geometry. The model consists of a rectangular basin that extends from the Northern Hemisphere across the equator and connects to a circumpolar channel south of 40°S. (b) The bottom topography is shown as the black shaded region. A topographic ridge is centered at 60°E, rising to a depth of 2000 m with a longitudinal width of 10°. The model has a sloping bottom west of 10°E and east of 50°E. Periodic boundary conditions are used to the south of 40°S. The gray region is the continental boundary (coast) for the basin north of 40°S.

eters together with the estimate of α and $\bar{\Psi}$, we find that $\phi = 10$, much greater than unity. It suggests that the simplified relationship of Eq. (17) may be appropriate. This is equivalent to assuming that wind-driven Eulerian-mean circulation contributes relatively little to this particular overturning circulation. In this case, the magnitude of the residual-mean circulation is proportional to $\sqrt{\kappa K}$. Eddy-induced circulation drives northward transport in the lower limb, which is partially compensated for by the southward transport of the Eulerian-mean circulation. If $\phi \sim O(10)$, some compensation is expected in Eq. (14) between $\bar{\Psi}$ and Ψ^* , with a net significant northward transport.

Diapycnal diffusivity and the mesoscale eddy transfer coefficient are not yet well quantified in the region, so it is difficult to determine the exact magnitude of ϕ . Marshall and Radko (2006) estimated the near-surface, isopycnal eddy diffusivity in the range of 500–2000 $\text{m}^2 \text{s}^{-1}$. Significant regional variability of K is expected while the overall magnitude of K in the deep Southern Ocean may be somewhat smaller than the near-surface values. Inverse modeling studies of Ganachaud and Wunsch (2000) inferred globally averaged κ between 3 and $12 \times 10^{-4} \text{m}^2 \text{s}^{-1}$. Based on these estimates, ϕ may vary from 10 to 140. Assuming a zonal length scale of the circumpolar ocean, $L_X = 2.8 \times 10^7 \text{m}$, the intensity of the lower-limb circulation is then in the range of 4 to 15 (Sv) ($1 \text{ Sv} \equiv 10^6 \text{m}^3 \text{s}^{-1}$), which is in general accord with estimates based on inverse models and geochemical tracers. However, significant uncertainty and variability of κ and K imply that the magnitude of ϕ is

highly uncertain, and so we must interpret these numbers as provisional.

3. Test of the scaling with a numerical ocean model

We now wish to evaluate the degree to which the ideas developed in the previous section help us to understand the sensitivities of the lower-limb circulation in a more complicated, three-dimensional circulation model. To do this, we use the Massachusetts Institute of Technology ocean general circulation model (MITgcm) (Marshall et al. 1997a,b). In particular, we examine the sensitivity of lower-limb circulation to perturbations in diapycnal diffusivity and eddy transfer coefficient. We first describe the control simulation in which the model is spun up to a steady state and examine simulated transport fields. In the sensitivity experiments, physical parameters are modified and the model is spun up again. The steady-state responses are then compared with the control simulation.

The numerical model is configured for a rectangular basin connected to a zonal channel at a coarse resolution ($2^\circ \times 2^\circ$, 30 vertical levels) similar to the model used in Ito and Deutsch (2006). The domain extends from 60°S to 60°N across 60° of longitude and uses periodic boundary condition for the circumpolar channel between 40° and 60°S (see the schematic diagram in Fig. 3a). The bathymetry of the model includes a topographic ridge below 2000-m depth as shown in Fig. 3b. The thickness of the vertical layers is set to 50 m for the

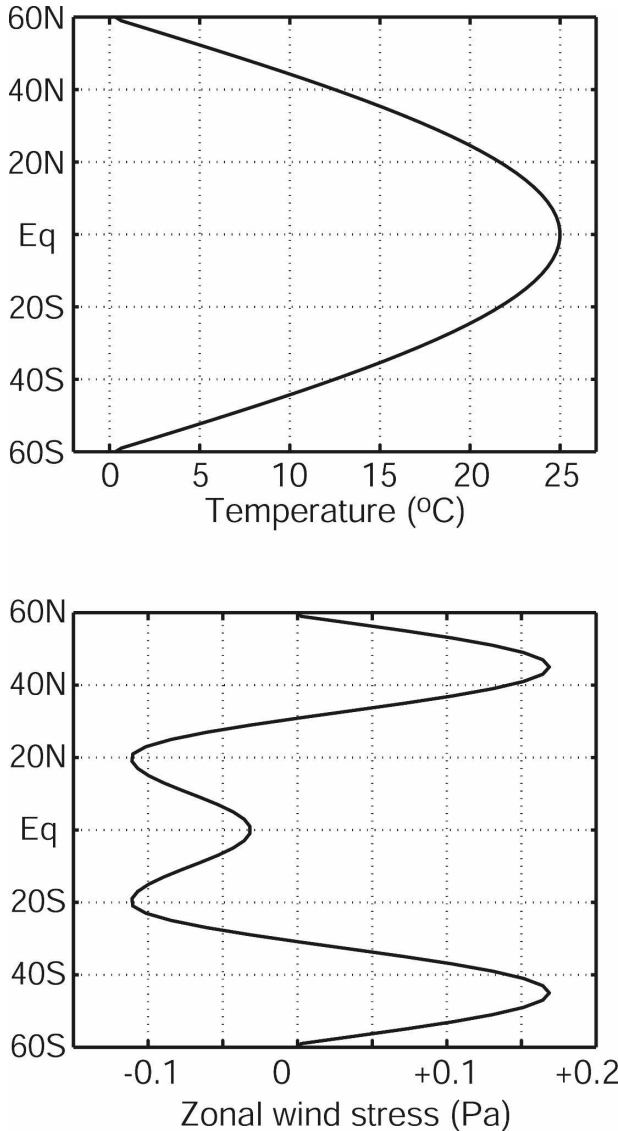


FIG. 4. Idealized forcing of the numerical model. (top) Surface boundary condition for temperature and (bottom) zonal wind stress. SST and wind stress do not vary in longitude.

top 5 layers, 100 m for the next 20 layers, and 150 m for the bottom 5 layers. Sea surface temperature (SST) is restored to a cosine profile with a time scale of 30 days (Fig. 4). An idealized zonal wind stress is applied to the surface ocean. For simplicity, there is no seasonal variation in the model, and salinity is set to a uniform constant. The model is initialized from a state of rest and uniform temperature and is spun up over 3000 yr of integration until the model reaches a steady state.

a. Control run

In the control run, diapycnal mixing is parameterized following Bryan and Lewis (1979) in which vertical dif-

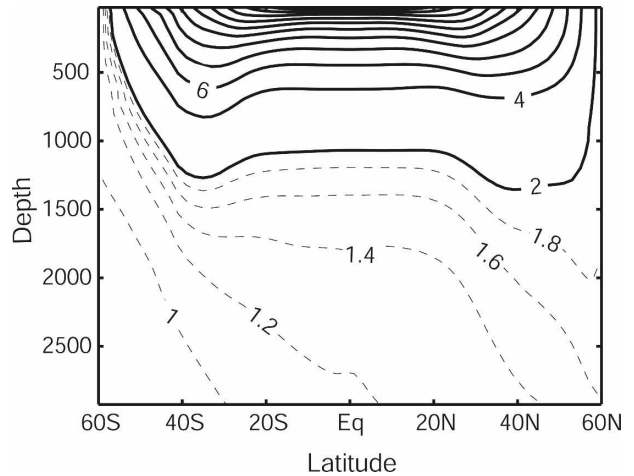


FIG. 5. Zonally averaged temperature at steady state in the control run. The contour interval of the solid lines is 2°C and that of the dashed lines is 0.2°C.

fusivity is set to $0.3 \times 10^{-4} \text{ m}^2 \text{ s}^{-1}$ in the upper ocean and increases to $1.0 \times 10^{-4} \text{ m}^2 \text{ s}^{-1}$ below a depth of 2000 m. Mesoscale eddy fluxes are parameterized using the isopycnal thickness diffusion scheme (GM90) in which the eddy transfer coefficient is set to a uniform value of $1000 \text{ m}^2 \text{ s}^{-1}$.

The modeled physical transport and buoyancy distribution are diagnosed for the steady-state solution. Figure 5 shows the simulated, zonally averaged temperature distribution from the control run. The buoyancy distribution is determined by the temperature only, because salinity is set to a uniform constant value. The temperature distribution indicates that deep waters colder than 1.8°C outcrops in the Southern Hemisphere only, indicating that they are formed in the southern high latitudes in this particular model. Those isopycnal surfaces generally intersect the bottom topography at all longitudes in the deep ocean. The densest water is found in the circumpolar channel, and the isopycnal slope is steep throughout the water column in this region.

Figure 6 shows the modeled meridional overturning circulation (MOC). The residual-mean circulation (Ψ_{res} shown in the bottom of Fig. 6) is the sum of the Eulerian-mean ($\bar{\Psi}$ shown in the top of Fig. 6) and the eddy-induced circulation (Ψ^* shown in the middle of Fig. 6). We define streamfunctions by vertically integrating the meridional velocity upward from the bottom:

$$\Psi(y, z) = - \int_0^{L_x} \int_{-H}^z v \, dz \, dx, \quad (18)$$

where L_x is the zonal width of the model domain. These calculations are carried out in spherical coordinates.

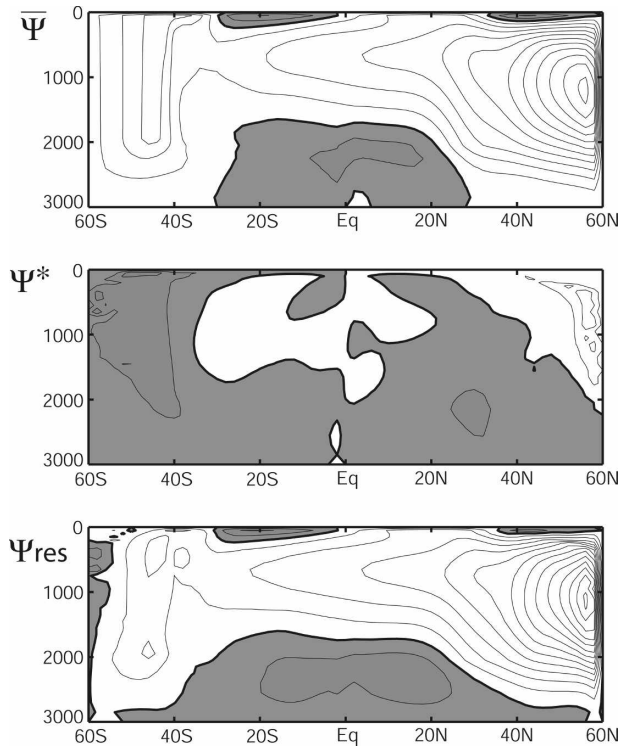


FIG. 6. Simulated MOC in the control run. (top) Eulerian-mean circulation $\bar{\Psi}$, (middle) eddy-induced circulation Ψ^* , and (bottom) residual-mean circulation Ψ_{res} . The thick solid lines represent $\Psi = 0$. The shaded regions represent negative values. Contour interval is 2 Sv.

Deep water formation in the Northern Hemisphere is dominated by the Eulerian-mean overturning circulation, where approximately 20 Sv of deep water is formed. In the circumpolar channel, the sign of $\bar{\Psi}$ (Fig. 6 top) and Ψ^* (Fig. 6 middle) is different.

The Eulerian-mean streamfunction is vertically oriented in the circumpolar channel above the depth of the bottom topography (2000-m depth), as predicted by our simple theory. Its magnitude is in excellent agreement with Eq. (8), which predicts that the magnitude of $\bar{\Psi}$ is set by the surface wind stress. For example, the wind stress of 0.15 Pa will support 5.8 Sv of $\bar{\Psi}$ at 50°S.² Below the depth of the bottom topography, $\bar{\Psi}$ gradually declines downward due to the mountain drag and associated poleward transport.

Eddy-induced circulation takes on a sign opposite to that of the Eulerian mean, partially canceling out the wind-driven overturning. In contrast to the Eulerian-mean circulation, the eddy-induced circulation does not

weaken below the depth of the topographic ridge in the circumpolar channel. As a consequence, the cancellation between $\bar{\Psi}$ and Ψ^* becomes more complete there.

Near the surface, the wind-driven upwelling of the deep water (~ 6 Sv) is partially compensated for by the eddy-induced circulation (~ -3 Sv). Thus, the residual-mean circulation, the sum of $\bar{\Psi}$ and Ψ^* , is primarily driven by the Eulerian-mean circulation, and its magnitude is on the order of 3 Sv. Below the depth of the topographic ridge, the deep meridional overturning circulation does not appear very clearly in this particular calculation, where the residual-mean circulation becomes very close to 0 below 2000-m depth. Although the background magnitude of Ψ_{res} is relatively small in the control run, we find significant sensitivity of Ψ_{res} to model parameters, as we discuss in the following sections.

b. Sensitivity experiments

We examine a series of sensitivity experiments by perturbing model parameters and evaluating the sensitivity of the lower-limb circulation. The perturbation runs are initialized with the spunup state of the control and then integrated for an additional 2000 yr to reach new steady states. We systematically vary vertical diffusivity (κ) and mesoscale eddy transfer coefficient (K) in the two series of model runs (see Fig. 7). We first discuss the response to variations in κ and K separately and go on to demonstrate that our results can be interpreted using the simple conceptual model in a consistent way.

1) EXPERIMENT 1: SENSITIVITY OF Ψ_{res} TO THE DIAPYCNAL MIXING

In experiment 1, vertical diffusivity (κ) is perturbed over a range between $1.0 \times 10^{-4} \text{ m}^2 \text{ s}^{-1}$ (control) and $6.0 \times 10^{-4} \text{ m}^2 \text{ s}^{-1}$ in the deep ocean, keeping all the other parameters unchanged. The profile of κ smoothly changes from unperturbed surface value ($0.3 \times 10^{-4} \text{ m}^2 \text{ s}^{-1}$) to abyssal values at 2000-m depths. The vertical variation is mathematically determined following the parameterization of Bryan and Lewis (1979).

Figure 8 shows the difference in the meridional overturning circulations between the control run and the perturbation experiments. We are primarily interested in the response of the residual-mean circulation. The change in Ψ_{res} is broken down into Eulerian-mean ($\bar{\Psi}$) and eddy-induced (Ψ^*) components.

The strongest response in Ψ_{res} occurs below 2000 m in the depth range where κ is perturbed: as κ increases, the lower-limb circulation intensifies. The Eulerian-mean circulation is insensitive to the variation in κ in all model runs. It is consistent with the theoretical predic-

² Interpreting the magnitude of the overturning circulation. Recall that our model represents a sector of the longitudinal width of 60°, only 1/6 of the globe.

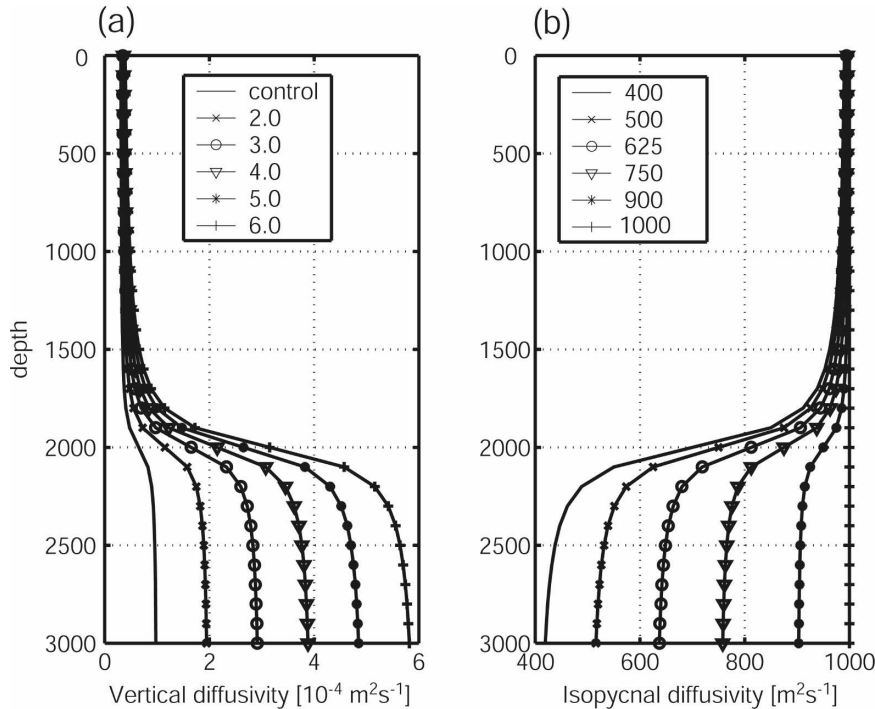


FIG. 7. Vertical profile of (a) vertical diffusivity and (b) eddy transfer coefficient employed in the sensitivity experiments.

tion that $\bar{\Psi}$ reflects the action of surface wind stress and topographic drag as expressed in the simple model in Eq. (8). Thus, changes in Ψ_{res} are primarily associated with changes in the eddy-induced circulation. The parameterized eddy fluxes depend on the slope of isopycnal surfaces, which is perturbed by the changes in κ .

Here, we examine the response of the lower-limb circulation in detail, using the diagnosed physical parameters. To test the scaling theory, we will diagnose the regionally averaged Ψ_{res} as a measure of the intensity of the lower-limb circulation. The amplitude of the lower limb is diagnosed by taking the average of Ψ in the latitude range of 50° and 30° S below 2500-m depth. The depth range is chosen such that the effect of the vertical gradient of κ is negligible, and the model fields then have a chance of being consistent with the assumptions made in the theory.

Figure 9 shows the dependence of $\bar{\Psi}$, Ψ^* , and Ψ_{res} on κ . In the control run, $\bar{\Psi}$ and Ψ^* are close to a complete cancellation. As κ increases, Ψ^* becomes more dominant and the variation of Ψ_{res} is almost all due to intensification of Ψ^* .

Our theory predicts a simple relationship between Ψ_{res} and κ through the buoyancy balance in Eqs. (11) and (13), which can be tested against simulated model fields. We first diagnose the scale height (z_0) and the meridional length scale (L) from the sensitivity runs.

The scale height of the buoyancy distribution can be calculated from the vertical profile of buoyancy:

$$z_0 = z \left\{ \ln \left[\frac{b(z)}{b_0} \right] \right\}^{-1}, \tag{19}$$

where $b(z)$ is the horizontally averaged vertical buoyancy profile in the latitude range over which Ψ_{res} is averaged (between 50° and 30° S) and b_0 is the mean surface value in the region. We obtain a vertical profile of z_0 , which varies from about 800 m in the thermocline to about 1100 m in the deep ocean. The magnitude of z_0 does not vary significantly between our model runs. Below the depth of 2500 m, z_0 remains approximately 1100 m, regardless of the magnitude of κ .

The meridional length scale (L) is evaluated for the isopycnal layer that passes through 50° S at a depth of 2500 m by calculating the distance between 50° S and the latitude where the layer intersects the bottom topography. The diagnosed values for L from the model runs covary with the magnitude of the isopycnal slope (s_p) in the region. Here, L significantly decreases with higher κ due to an increased isopycnal slope. The variation of the aspect ratio (z_0/L) is primarily controlled by the variation of L , and it is found to vary linearly with the isopycnal slope. The dimensionless parameter, α in Eq. (13), can be determined by taking the ratio of (z_0/L) to s_p from its definition in Eq. (12).

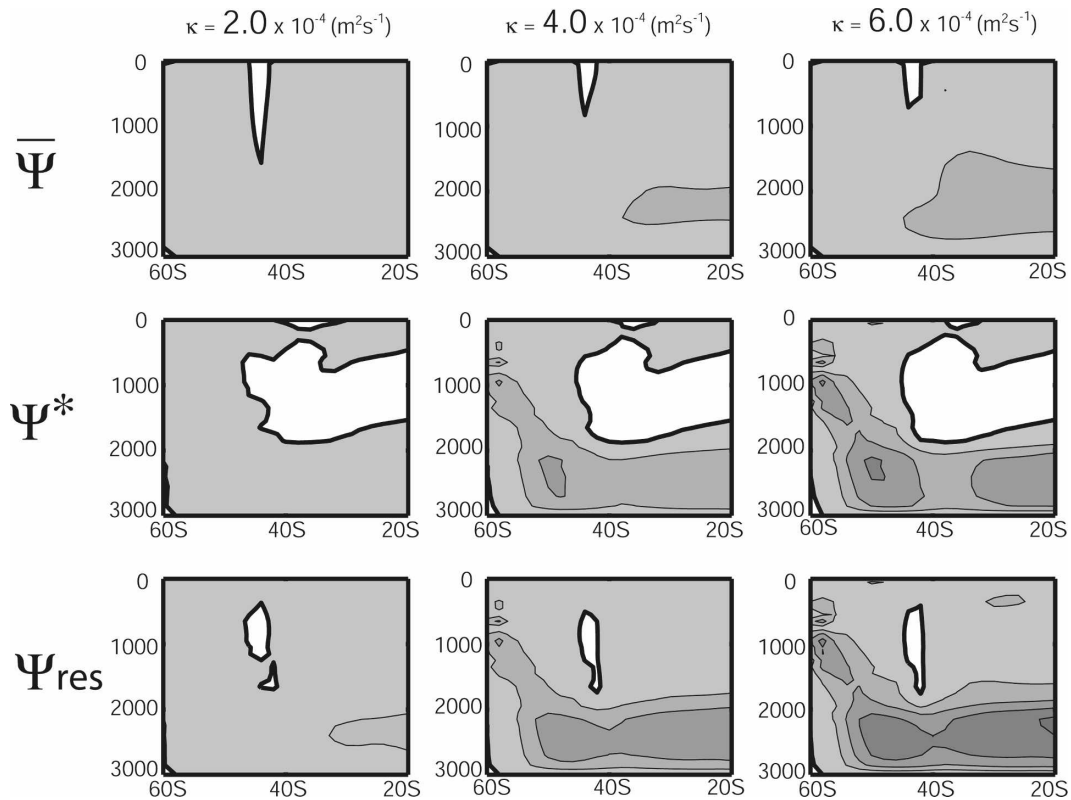


FIG. 8. Perturbations in Ψ are plotted from the sensitivity experiments with varying κ . The magnitude of the perturbation is calculated by taking the difference in Ψ between the sensitivity experiments and the control run. (left to right) The abyssal κ increases from $2.0 \times 10^{-4} \text{ m}^2 \text{ s}^{-1}$ to $4.0 \times 10^{-4} \text{ m}^2 \text{ s}^{-1}$ and $6.0 \times 10^{-4} \text{ m}^2 \text{ s}^{-1}$. (top) The perturbation in the Eulerian-mean circulation ($\bar{\Psi}$). (middle, bottom) The eddy-induced circulation (Ψ^*) and the residual circulation (Ψ_{res}), respectively. The thick solid lines represent zero, and the shaded regions represent negative values. The contour interval is 0.5 Sv.

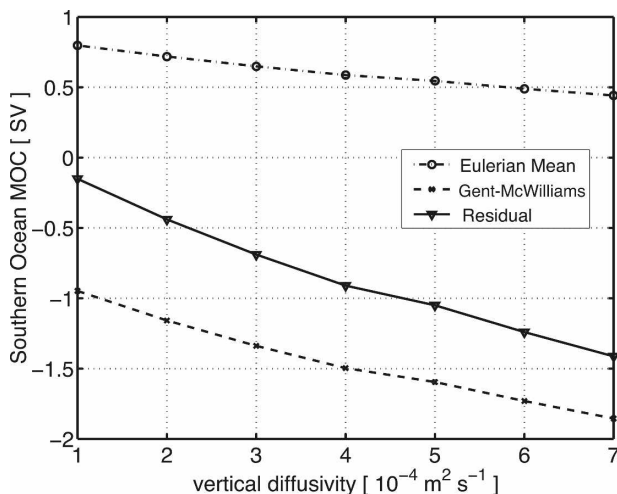


FIG. 9. The response of the regionally averaged meridional overturning circulation from experiment 1. The horizontal axis is the prescribed vertical diffusivity in the deep ocean. The three lines represent $\bar{\Psi}$ (dashed-dotted, “Eulerian mean”), Ψ^* (dash, “Gent-McWilliams”), and Ψ_{res} (solid, “residual”).

For this particular set of experiments, the best fit value for α is found to be about 0.13. Given α we can evaluate the relationship [Eq. (13)] by comparing the simulated $\Psi_{\text{res}} s_{\rho} \alpha^{-1}$ to the corresponding κ . Figure 10 shows that this theoretical prediction is generally consistent with the results from experiment 1. The isopycnal slope and Ψ_{res} both increase with κ , and their relationship is determined by the dimensionless number, α . Now that we have established the simple relationship between Ψ_{res} , s_{ρ} , and κ , it follows that the intensity of Ψ_{res} can be determined in terms of the dimensionless number, ϕ , which is a combination of α , κ , K , and $\bar{\Psi}$. We will use this concept later to unify the results from all sensitivity experiments and draw them all into a consistent framework.

2) EXPERIMENT 2: SENSITIVITY OF Ψ_{res} TO THE EDDY TRANSFER COEFFICIENT

In experiment 2, we perturb the isopycnal eddy transfer coefficient, keeping all the other parameters constant. The profile of K is perturbed as shown in Fig. 7b.

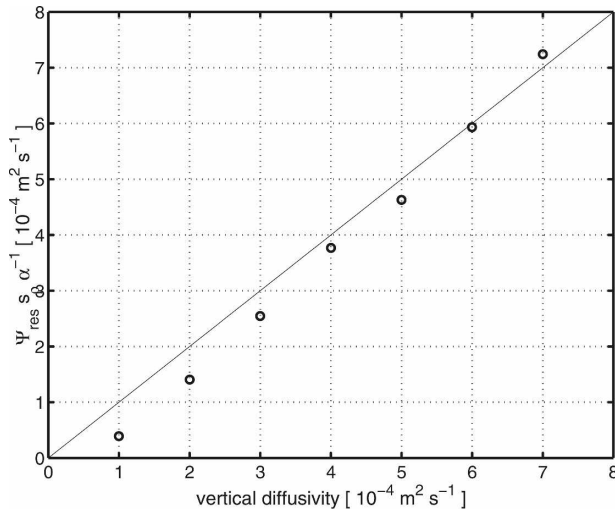


FIG. 10. Testing the theoretical prediction, Eq. (13). The horizontal axis is the prescribed vertical diffusivity (κ) from each sensitivity run, and the vertical axis is the diagnosed values for $\Psi_{\text{res}} s_{\rho} \alpha^{-1}$. The solid line represents the theoretical prediction, $\Psi_{\text{res}} s_{\rho} \alpha^{-1} = \kappa$.

In the control run, K is held constant throughout the water column. Here, we vary the magnitude of abyssal K over a range between 400 and 1000 $\text{m}^2 \text{s}^{-1}$. The assumed vertical profile has a smooth transition from the unperturbed upper ocean to the deep ocean at a depth of 2000 m. The model is initialized with the steady state of the control run, and then spun up to another steady state with the perturbed K . In this series of experiments, abyssal vertical diffusivity (κ) is set to $4 \times 10^{-4} \text{m}^2 \text{s}^{-1}$.

Figure 11 shows the difference in the meridional overturning circulations between the control run and a subset of our perturbation experiments. As with experiment 1, we examine the response of the residual-mean circulation and its two components. The strongest response in Ψ_{res} occurs below 2000-m depth where K is perturbed. The Eulerian-mean circulation is insensitive to the variation in K because, as already discussed, it is primarily controlled by the surface wind stress. The response of the residual circulation to the variations in K is determined by the eddy-induced circulation. As K increases, the lower limb Ψ_{res} becomes stronger.

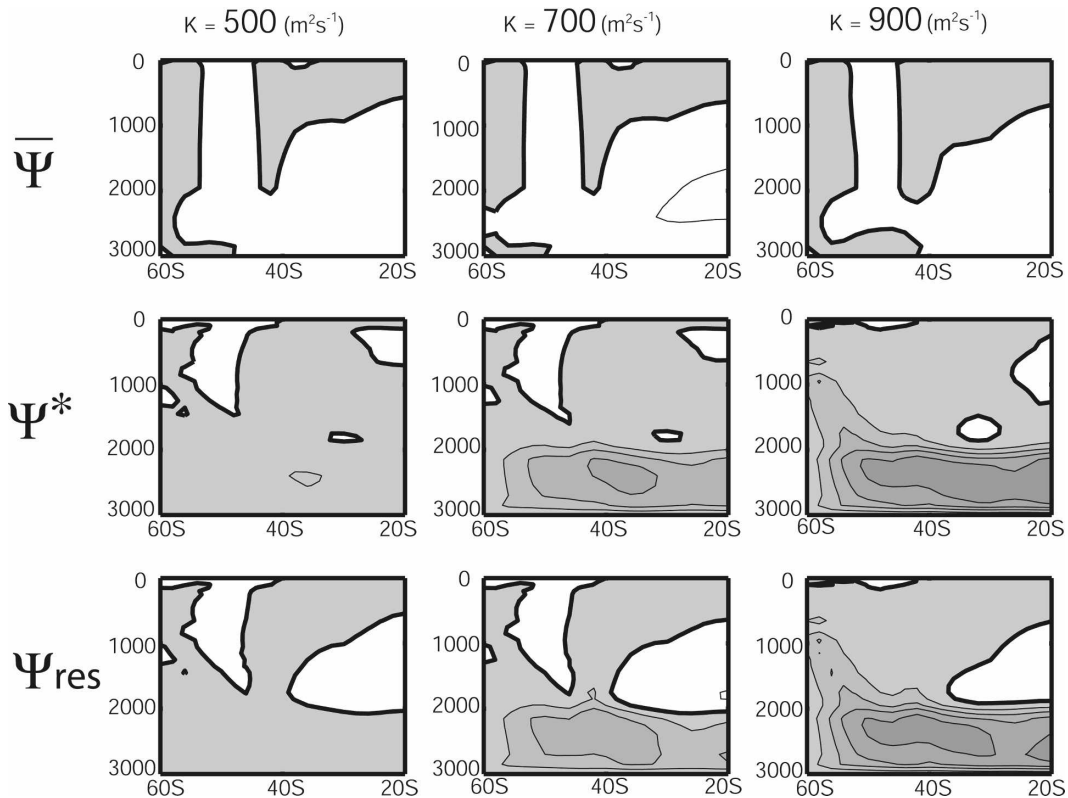


FIG. 11. Perturbations in Ψ are plotted from the sensitivity experiments for different values of K . The magnitude of the perturbation is calculated by taking the difference between the sensitivity experiments and the control run. (left to right) Here K increases from 500 to 750 $\text{m}^2 \text{s}^{-1}$ and 900 $\text{m}^2 \text{s}^{-1}$. (top) The perturbation in the Eulerian-mean circulation ($\bar{\Psi}$). (middle, bottom) The eddy-induced circulation (Ψ^*) and the residual circulation (Ψ_{res}), respectively. The thick solid lines represent zero. Shaded regions represent negative values. Contour interval is 0.2 Sv.

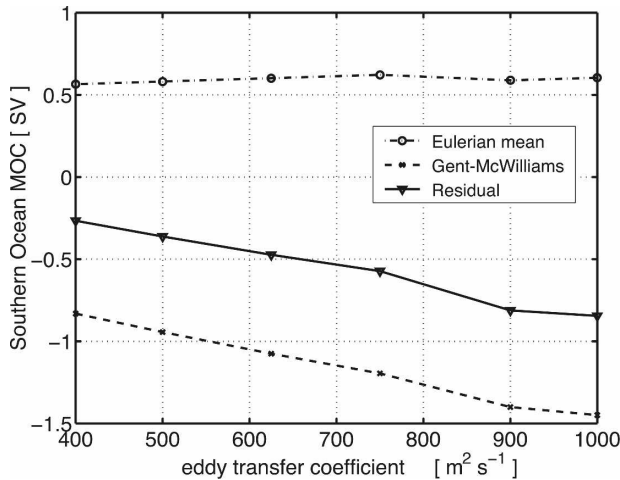


FIG. 12. The response of the meridional overturning circulation averaged below a depth of 2500 m between 50° and 30°S from experiment 2. The horizontal axis is the magnitude of the eddy transfer coefficient in the deep ocean. The three lines represent Ψ (dashed-dotted), Ψ^* (dash), and Ψ_{res} (solid).

Here, we examine the quantitative relationship between K and the strength of the lower limb. As in experiment 1, the amplitude of the lower limb is evaluated by taking the average of Ψ in the latitude range 50° and 30°S below a depth of 2500 m. The depth range is chosen such that the effect of the vertical gradient of K is negligible enabling the model to be compared with the theory. Figure 12 shows the dependence of the lower-limb circulation on K . As K increases, Ψ^* becomes more dominant and the variation of Ψ_{res} can be explained by the intensification of Ψ^* .

Equation (13) suggests that the changes in Ψ_{res} and s_ρ tend to cancel out when κ is held constant. This relationship can be readily tested by calculating the product of Ψ_{res} and s_ρ from the sensitivity experiments. When K increases, the lower-limb circulation becomes stronger and the magnitude of Ψ_{res} increases, as seen in Fig. 11. The increase in K tends to flatten isopycnal surfaces, and the magnitude of s_ρ decreases with greater K . These two effects partially cancel out, but the compensation is not complete, which is a deviation from the theoretical prediction, indicating that α is not exactly a constant. There is a minor residual due to the stronger increase in Ψ_{res} relative to s_ρ . Over the range of K used in this experiment, Ψ_{res} has increased by approximately a factor of 3, whereas the corresponding decrease in s_ρ is roughly a factor of 2. Given the simplicity of the theory, there could be many factors for the disagreement, as discussed later.

Sensitivity experiments show that the overturning circulation intensifies with greater abyssal K even in the presence of a flatter isopycnal surface. We now further

examine the response of the buoyancy structure to the variation of K . As in experiment 1, the scale height is diagnosed using the formula in Eq. (19). Again, the magnitude of z_0 is remarkably stable and does not change significantly with K throughout the model runs. Its magnitude is almost identical to that of experiment 1, approximately 1100 m. The meridional length scale (L) is also diagnosed using the same method. The magnitude of L covaries with the isopycnal slope in response to the changes in K . Here, L increases with greater K due to the flattening of isopycnal surfaces. Thus, the variation of the aspect ratio (z_0/L) is primarily controlled by the variation of L and is directly related to the variation of isopycnal slope. For this set of experiments, we find that $\alpha = 0.15$, not very different from the value in experiment 1. The magnitude of α only depends on the buoyancy structure of the deep ocean, and its magnitude remains within a small range (0.13–0.15) throughout all model runs, including sensitivity experiments 1 and 2.

c. Synthesis of model runs

Perturbations in κ and K have different manifestations in the buoyancy structure and circulation of the circumpolar ocean, and yet together they influence the intensity of the meridional overturning circulation. We now discuss combined results from experiments 1 and 2, and we interpret them in the light of our simple theory.

Our theory predicts that the magnitude of Ψ_{res} is ultimately determined by the dimensionless parameter, ϕ , which combines the magnitude of κ , K , and $\bar{\Psi}$. We now use this relationship to bring together the results from all of the sensitivity runs. Figure 13 shows the excellent agreement with the theory [as encapsulated in Eq. (15)]. The relationship between Ψ_{res} and ϕ diagnosed from all of the sensitivity experiments collapses on to the relationship predicted by the simple theory. Inspection of the horizontal axis of Fig. 13 shows that the magnitude of ϕ can be significantly larger than 1, in particular when κ or K is relatively large. Equation (17) suggests that Ψ_{res} is proportional to $\sqrt{\kappa K}$ and the constant of proportionality is equal to the square root of α . We find that this simplified relationship can also give a reasonably good prediction for the sensitivity of Ψ_{res} . The results from the model runs approach the limit of Eq. (17) when the magnitude of κK is sufficiently large in accord with our theory.

4. Discussion and conclusions

The meridional overturning circulation in the Southern Ocean consists of two overturning cells: the upper

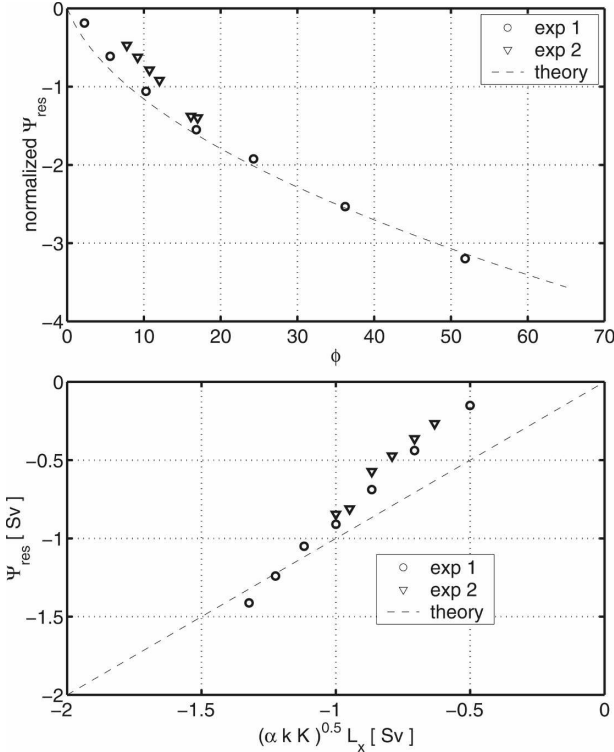


FIG. 13. Synthesizing the results from experiments 1 and 2. (top) The solid line shows the theoretical prediction of the relationship between Ψ_{res} and ϕ as given by Eq. (15). The circular dots represent the results from experiment 1, and the triangular dots represent the results from experiment 2. (bottom) The simplified relationship between Ψ_{res} and $\sqrt{\kappa K}$, as given by Eq. (17). The magnitude of the volume flux is calculated by multiplying by the zonal length of the circumpolar channel (L_x).

limb and the lower limb. Recent observational studies (Heywood et al. 2002; Naveira Garabato et al. 2004; 2007) have shown the existence of intense diapycnal mixing near the bottom topography of the Southern Ocean. In this paper, we have hypothesized that elevated levels of diapycnal diffusivity (κ) play an important role in the buoyancy balance of the lower-limb circulations, and we developed a simple theory building on residual-mean theory.

a. Scaling theory

Diapycnal mixing must be invoked to balance cross-isopycnal mass flux by the residual-mean flow. Integrating the buoyancy balance over the bottom layer where κ is elevated, we find a simple, diagnostic relationship, $\Psi_{\text{res}} s_\rho \propto \kappa$, indicating that the product of the lower-limb circulation and the isopycnal slope is proportional to the diapycnal diffusivity. Physically, this relationship indicates that the overturning circulation must balance

buoyancy forcing due to diapycnal mixing, and the intensity of Ψ_{res} is proportional to κ if the isopycnal slope (s_ρ) is prescribed. In reality, changes in κ will also impact the buoyancy structure and so we must also take into account the variation of s_ρ .

Numerical experiments suggest that changes in the lower-limb circulation is primarily associated with the eddy-induced circulation, $\Psi_{\text{res}} \sim \Psi^* = K s_\rho$, where the second part of the equality is based on the eddy closure of (GM90). Combining with $\Psi_{\text{res}} s_\rho \propto \kappa$, we find a simple scaling relation for the intensity of the lower limb, $\Psi_{\text{res}} \propto \sqrt{\kappa K}$. This relationship has been tested against a suite of numerical simulations. The simulated response of Ψ_{res} is primarily due to changes in Ψ^* at the depths where κ is perturbed, here below the depth of the modeled bottom topography, consistent with this heuristic derivation. Note that the sensitivity of Ψ_s depends on the eddy closure employed for Ψ^* ; for example, the parameterization of Visbeck et al. (1997) suggests $\Psi^* = k s_\rho^2$, which would lead to a different sensitivity of $\Psi_{\text{res}} \propto \sqrt[3]{\kappa}$.

b. Relation to the upper-limb circulation

Our study has focused on the effect of intense diapycnal diffusivity in the abyssal Southern Ocean, assuming that the upper ocean processes remain unchanged. However, interactions with the upper limb may introduce additional factors that suggest extensions of our theory.

The dynamics of the upper-limb circulation primarily determines the upper ocean pycnocline depth (i.e., the scale height z_0), which may affect the abyssal density structure and the lower-limb circulation. Stronger eddy stirring (or equivalently weaker zonal wind stress) in the upper ocean leads to a shallower pycnocline (Gnanadesikan 1999; Karsten et al. 2002; MR03), which tends to decrease z_0 . In the limit of small residual circulation, z_0 scales as the inverse of upper ocean eddy transfer coefficient ($z_0 \propto K^{-1}$). A change in scale height z_0 can thus modulate the abyssal isopycnal slope because $s_\rho \sim \alpha z_0/L$, where L is the meridional scale of AABW and α is a constant scale factor. Numerical experiments suggest that the magnitude of L scales as the square root of abyssal eddy transfer coefficient ($L \propto K^{1/2}$) in experiment 2. If the eddy transfer coefficient K is perturbed throughout the water column and the responses of s_ρ to changes in z_0 and L are independent, the combined effect may lead to more effective flattening of isopycnal layers, $s_\rho \propto K^{-3/2}$. In this case, the lower-limb circulation can be weakened rather than strengthened by the enhanced eddy stirring in the upper ocean, $\Psi_{\text{res}} \propto K^{-1/2}$.

Furthermore, Kamenkovich and Goodman (2000)³ consider a scenario in which the lower-limb circulation adjusts to upper ocean mixing. They argue that increasing diapycnal mixing in the full water column will impact abyssal circulation through two processes. First, increased upper ocean mixing deepens the upper ocean thermocline, which will make the bottom layer thinner due to the geometrical constraint, leading to a weaker lower-limb circulation. Second, increased upper ocean mixing will increase the meridional density gradient of the deep ocean, leading to a stronger lower-limb circulation. These two processes compete with one another. In their particular numerical experiments, the second mechanism dominates the response of lower-limb circulation. To fully elucidate the interactions with the upper ocean processes, abyssal mixing, and the eddies in the Southern Ocean, we must also consider possible interactions between the upper- and lower-limb circulation, thermocline depth, and abyssal density structures, a topic that is left for the future study.

c. Energy source for mixing

Turbulent mixing in the stratified water column will raise the center of mass and so requires a continuous input of energy. It has been speculated (Wunsch and Ferrari 2004) that the energy source for enhanced dissipation may ultimately come from the tidal currents and/or surface wind stress. Residual mean theory of the zonal momentum balance suggests that ocean eddies play a central role in the vertical transfer of zonal momentum (Andrews and McIntyre 1976), which may control the pathway of momentum and energy from the surface winds to the bottom topographic drag through interfacial form stress (Johnson and Bryden 1989). The coupling between surface wind stress and ocean eddies primarily controls the density structure and the zonal geostrophic current of the ACC through thermal wind balance (Karsten et al. 2002). Enhanced diapycnal mixing in the abyssal Southern Ocean may be associated with the rough topography, indicating the possible role of the interaction of the ACC with the bottom topography, which excites inertia-gravity waves and provides a route to mixing (Naveira Garabato et al. 2004). Therefore, the strength of surface winds, eddy stirring, and abyssal mixing are likely to depend on one another. In this study, to make progress, we have implicitly assumed that these processes are independent of one another, as is current practice in ocean models. However, there may be important dynamical couplings between

τ_s , K , and κ . Improved understanding of the interactions between these parameters may modify our theoretical predictions and scalings, which is clearly an important area for future study.

d. Caveats and suggestion for future study

This study used highly idealized models of the Southern Ocean to better understand aspects of the complicated system. In addition to the above discussion, further simplifying assumptions are the subject of continuing study. First, the simple model presented here builds on the f -plane theory of MR03 in which there is no account taken of the β effect. The remarkable agreement between the theoretical predictions and the numerical sensitivity experiments suggests that the f -plane theory is indeed sufficient to describe the leading-order balance in the ACC [see also the appendix of Marshall and Radko (2006) where β effects are discussed]. However, the eddy closure (GM90) is an f -plane parameterization adopted both in the analytical and the numerical calculations. It may break down in the ACC, where β and topographic β constraints are likely to be important. Further study is required to examine such effects.

Second, the geometry of the model is highly idealized and the results must therefore be interpreted with caution. Furthermore, deep water formation processes are not explicitly represented in our model. Instead, we have focused on the dynamical balances that control the flux of dense Antarctic Bottom Water to the interior ocean. Further investigation is required to link the ventilation of deep waters near the Antarctic continent and the formation of bottom water. Finally, one further limitation of our theory is the focus on the dynamics related to the circumpolar channel. For example, Gnanadesikan (1999) relates the dynamics of the upper-limb circulation to the global meridional overturning circulation through the global adjustment of the pycnocline. The lower-limb circulation is connected to the northern basins, which are governed by different dynamics. Here, we have studied the lower-limb circulation somewhat in isolation. Ultimately, however, a global synthesis must emerge.

Acknowledgments. JM acknowledges support of the Polar Program division of NSF. TI is thankful for the support from NSF (Grant OCE-0647979) and NASA (Grant NNX08AL72G). We thank two anonymous reviewers who provided useful comments.

REFERENCES

- Andrews, D., and M. McIntyre, 1976: Planetary waves in horizontal and vertical shear: The generalized Eliassen-Palm relation and the zonal mean acceleration. *J. Atmos. Sci.*, **33**, 2031–2048.

³ Note, however, that Kamenkovich and Goodman (2000) use a model with horizontal and vertical mixing schemes, and thus they are not working within a residual-mean framework.

- Bryan, K., and L. J. Lewis, 1979: A water mass model of the world ocean. *J. Geophys. Res.*, **84**, 2503–2517.
- Bryden, H. L., and S. A. Cunningham, 2003: How wind-forcing and air–sea heat exchange determine the meridional temperature gradient and stratification for the Antarctic Circumpolar Current. *J. Geophys. Res.*, **108**, 3275, doi:10.1029/2001JC001296.
- Conkright, M. E., R. A. Locarnini, H. E. Garcia, T. D. O'Brien, C. Stephens, and J. I. Antonov, 2002: *World Ocean Atlas 2001: Objective analyses, data statistics, and figures*, CD-ROM documentation. National Oceanographic Data Center, Internal Rep. 17, 21 pp.
- Ganachaud, A., and C. Wunsch, 2000: Improved estimates of global ocean circulation, heat transport and mixing from hydrographic data. *Nature*, **408**, 453–457.
- Gent, P. R., and J. C. McWilliams, 1990: Isopycnal mixing in ocean circulation models. *J. Phys. Oceanogr.*, **20**, 150–155.
- Gille, S. T., 1997: The Southern Ocean momentum balance: Evidence for topographic effects from numerical model output and altimeter data. *J. Phys. Oceanogr.*, **27**, 2219–2232.
- Gnanadesikan, A., 1999: A simple predictive model for the structure of the oceanic pycnocline. *Science*, **283**, 2077–2079.
- Heywood, K. J., A. C. Naveira Garabato, and D. P. Stevens, 2002: High mixing rates in the abyssal Southern Ocean. *Nature*, **415**, 1011–1014.
- Ito, T., and C. Deutsch, 2006: Understanding the saturation state of argon in the thermocline: The role of air–sea gas exchange and diapycnal mixing. *Global Biogeochem. Cycles*, **20**, GB3019, doi:10.1029/2005GB002655.
- Ivchenko, V. O., K. J. Richards, and D. P. Stevens, 1996: The dynamics of the Antarctic Circumpolar Current. *J. Phys. Oceanogr.*, **26**, 753–774.
- Johnson, G., and H. L. Bryden, 1989: On the size of the Antarctic Circumpolar Current. *Deep-Sea Res.*, **36**, 39–53.
- Kamenkovich, I., and P. Goodman, 2000: The dependence of the AABW formation on vertical diffusivity. *Geophys. Res. Lett.*, **27**, 3739–3742.
- Karsten, R., and J. Marshall, 2002: Constructing the residual circulation of the ACC from observations. *J. Phys. Oceanogr.*, **32**, 3315–3327.
- , H. Jones, and J. Marshall, 2002: The role of eddy transfer in setting the stratification and transport of a Circumpolar Current. *J. Phys. Oceanogr.*, **32**, 39–54.
- Marshall, D., 1997: Subduction of water masses in an eddying ocean. *J. Mar. Res.*, **55**, 201–222.
- Marshall, J., and T. Radko, 2003: Residual-mean solutions for the Antarctic Circumpolar Current and its associated overturning circulation. *J. Phys. Oceanogr.*, **33**, 2341–2354.
- , and —, 2006: A model of the upper branch of the meridional overturning circulation of the Southern Ocean. *Prog. Oceanogr.*, **70**, 331–345.
- , A. Adcroft, C. Hill, L. Perelman, and C. Heisey, 1997a: A finite-volume, incompressible Navier–Stokes model for studies of the ocean on parallel computers. *J. Geophys. Res.*, **102**, 5753–5766.
- , C. Hill, L. Perelman, and A. Adcroft, 1997b: Hydrostatic, quasi-hydrostatic, and nonhydrostatic ocean modeling. *J. Geophys. Res.*, **102**, 5733–5752.
- Munk, W., 1966: Abyssal recipes. *Deep-Sea Res.*, **13**, 707–730.
- Naveira Garabato, A. C., K. L. Polzin, B. A. King, K. J. Heywood, and M. Visbeck, 2004: Widespread intense turbulent mixing in the Southern Ocean. *Science*, **303**, 210–213.
- , D. P. Stevens, A. J. Watson, and W. Roether, 2007: Short-circuiting of the overturning circulation in the Antarctic Circumpolar Current. *Nature*, **447**, 194–197.
- Olbers, D., and M. Visbeck, 2005: A model of the zonally averaged stratification and overturning in the Southern Ocean. *J. Phys. Oceanogr.*, **35**, 1190–1205.
- Phillips, H. E., and S. R. Rintoul, 2000: Eddy variability and energetics from direct current measurements in the Antarctic Circumpolar Current south of Australia. *J. Phys. Oceanogr.*, **30**, 3050–3076.
- Sloyan, B. M., and S. R. Rintoul, 2001: The Southern Ocean limb of the global deep overturning circulation. *J. Phys. Oceanogr.*, **31**, 143–173.
- Speer, K., S. R. Rintoul, and B. Sloyan, 2000: The diabatic Deacon cell. *J. Phys. Oceanogr.*, **30**, 3212–3222.
- Visbeck, M., J. Marshall, T. Haine, and M. Spall, 1997: On the specification of eddy transfer coefficients in coarse-resolution ocean circulation models. *J. Phys. Oceanogr.*, **27**, 381–402.
- Webb, D. J., and N. Sugihara, 2001: Oceanography: Vertical mixing in the ocean. *Nature*, **409**, 37, doi:10.1038/35051171.
- Wunsch, C., and R. Ferrari, 2004: Vertical mixing, energy, and the general circulation of the oceans. *Annu. Rev. Fluid Mech.*, **36**, 281–314.